Title
Mechanical Platelet Activation Potential in Abdominal Aortic Aneurysms

Journal
Journal of Biomechanical Engineering, 137(4)

ISSN
0148-0731

Authors
Hansen, Kirk B
Arzani, Amirhossein
Shadden, Shawn C

Publication Date
2015-04-01

DOI
10.1115/1.4029580

Peer reviewed

Mechanical Platelet Activation Potential in Abdominal Aortic Aneurysms

Kirk B. Hansen
Department of Mechanical Engineering,
University of California,
5126 Etcheverry Hall,
Berkeley, CA 94720-1740

Amirhossein Arzani
Department of Mechanical Engineering,
University of California,
5126 Etcheverry Hall,
Berkeley, CA 94720-1740

Shawn C. Shadden[1]
Department of Mechanical Engineering,
University of California,
5126 Etcheverry Hall,
Berkeley, CA 94720-1740
e-mail: shadden@berkeley.edu

Intraluminal thrombus (ILT) in abdominal aortic aneurysms (AAA) has potential implications to aneurysm growth and rupture risk; yet, the mechanisms underlying its development remain poorly understood. Some researchers have proposed that ILT development may be driven by biomechanical platelet activation within the AAA, followed by adhesion in regions of low wall shear stress. Studies have investigated wall shear stress levels within AAA, but platelet activation potential (AP) has not been quantified. In this study, patient-specific computational fluid dynamic (CFD) models were used to analyze stress-induced AP within AAA under rest and exercise flow conditions. The analysis was conducted using Lagrangian particle-based and Eulerian continuum-based approaches, and the results were compared. Results indicated that biomechanical platelet activation is unlikely to play a significant role for the conditions considered. No consistent trend was observed in comparing rest and exercise conditions, but the functional dependence of AP on stress magnitude and exposure time can have a large impact on absolute levels of anticipated platelet AP. The Lagrangian method obtained higher peak AP values, although this difference was limited to a small percentage of particles that falls below reported levels of physiologic background platelet activation. [DOI: 10.1115/1.4029580]

Keywords: abdominal aortic aneurysm, advection–diffusion-reaction, blood damage, computational fluid dynamics, Lagrangian particle tracking, platelet activation, thrombosis

1 Introduction

AAA disease is characterized by progressive, localized enlargement of the abdominal aorta. It is often accompanied by the growth of ILT, and ILT formation has been linked to both the progression [1] and risk of rupture [2] of AAA. The mechanisms of ILT formation, as well as the influence of ILT on AAA biomechanics, however, are complex and poorly understood [3,4].

Experimental [5–9] and numerical [6,7,10–13] studies have shown that AAA flow is often characterized by a core jet with a surrounding recirculation region. It has been hypothesized that ILT formation may be driven by stress-induced platelet activation and aggregation within the recirculation zone, followed by deposition in regions of low wall shear stress [6,10,14]. While several previous studies have investigated AAA wall shear stress levels [10,11,14–16], platelet activation levels within patient-specific AAA have not been reported.

Experiments have shown that biomechanical platelet activation is a function of both the magnitude and duration of applied stresses [17–19]. In a meta-analysis of previous experimental studies, Hellums et al. [20] plotted an activation locus that showed a power law relationship between threshold stress and exposure time, and Giersiepen et al. [21] developed a model based on similar results. These early experiments were conducted under constant shear conditions; application of the observed activation thresholds to more dynamic flow conditions experienced by platelets in vivo remains uncertain. Bluestein et al. [22] proposed that platelet activation level could be approximated by a linear stress-exposure time model. Later publications have used power law models to better reflect the results of experimental studies [23–26]. It has been shown that these models can give rise to mathematical and physical inconsistencies [27], although a more complex dose-based power law model has been developed to avoid these problems [28]. Recently, Soares et al. [29] and Sheriff et al. [30] have developed models that incorporate time history of stress, current stress, and rate of change of stress, and fit the model constants to experimental data covering a range of shear stress waveforms.

Previous studies of biomechanical platelet activation have typically modeled platelets as either infinitesimal [22,23,25,31–33] or finite-sized [26,34–38] particles. In either case, Lagrangian particle tracking of the position and stress histories of individual platelet surrogates in the flow is used. In the medium to large arteries, tens of millions to billions of platelets can pass through the artery each second [39], making direct tracking of physiological platelet counts computationally infeasible in such domains. Instead, some researchers have utilized an Eulerian framework, in which concentrations of activated platelets are tracked as a continuum quantity [40–44]. To date, these Eulerian frameworks have been applied to the *biochemical* activation of platelets, and use of such methods to investigate *biomechanical* activation has been less explored.

This study seeks to better quantify the potential for biomechanical platelet activation in AAA under different physiologic states, as well as potential discrepancies between continuum and discrete particle modeling of platelet transport. To this end, patient-specific CFD simulations were used to quantitatively investigate the potential for biomechanical platelet activation in AAA. Platelets were modeled using both Lagrangian particle tracking and Eulerian continuum approaches, and the results of these two methods were compared. Since hemodynamic conditions in a patient can vary considerably due to normal diurnal changes in physiology, and more specifically because lower-body exercise is a proposed therapy for patients suffering from AAA [45,46], both rest

[1]Corresponding author.

Manuscript received July 31, 2014; final manuscript received January 8, 2015; published online February 5, 2015. Assoc. Editor: Alison Marsden.

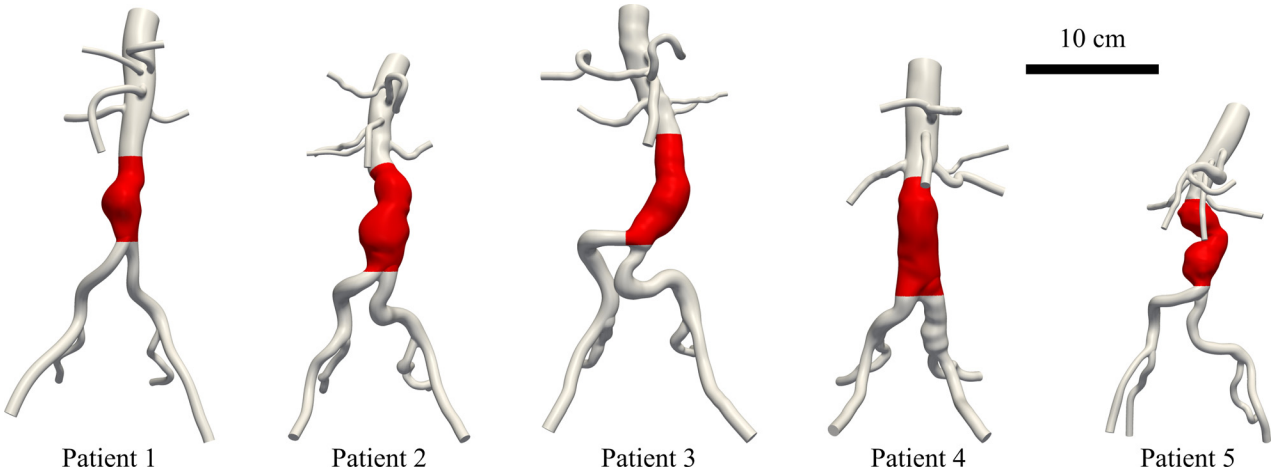

Fig. 1 Image-based computer models of the abdominal aorta and surrounding vasculature, with aneurysmal region of interest Ω highlighted in shade

and exercise hemodynamic conditions were considered. Moreover, although exercise has been shown to reduce particle residence time inside AAA [47], it also increases hemodynamic stress levels [11]. Since platelet AP depends on both stress magnitude and duration, and these two effects may counteract each other, numerical methods offer a powerful tool to investigate the net effect of complex hemodynamics on AP.

2 Methods

This study considered five patients with small AAA ($3\,\text{cm} < \text{dia} < 5\,\text{cm}$). Image-based CFD methods were used to obtain velocity fields within the abdominal aorta under rest and exercise conditions. These data were then postprocessed using Lagrangian and Eulerian computational techniques to determine platelet activation levels.

2.1 Image-Based CFD. The SIMVASCULAR software package[1] was used to construct three-dimensional models of the abdominal aorta and surrounding arteries from magnetic resonance imaging (MRI) angiography (cf. Fig. 1). The resulting geometric models were used as computational domains for simulation of blood flow dynamics. Blood was modeled as an incompressible, Newtonian fluid ($\rho = 1.06\,\text{gcm}^{-3}, \mu = 0.04\,\text{P}$) by the Navier–Stokes equations, which were solved using a stabilized finite element method [48,49].

The vessel wall was modeled as rigid with a no-slip boundary condition. For rest, patient-specific inflow boundary conditions were set by mapping two-dimensional phase-contrast (PC)-MRI data to a Womersley profile at the supraceliac aorta. The inflow boundary condition, and corresponding PC-MRI measurement, was chosen well upstream of the aneurysm to ensure that flow features developed in the aneurysm resulted from local vascular morphology in order to mitigate errors resulting from specification of the inflow profile. Three-element Windkessel models were applied at the outlets and tuned as described by Les et al. [11]. Briefly, infrarenal PC-MRI data was used to tune resistances so that physiological flow distribution between the aneurysm and suprarenal arteries (celiac, superior mesenteric, and renal arteries) was achieved. Capacitances were tuned so that the pressure pulse in the model fit the measured brachial pressure pulse.

For the exercise condition, boundary conditions were modified as described by Les et al. [11]. Namely, the duration of diastole was shortened to increase the heart rate by 50%, and outflow resistances were changed to impose a 444% increase in infrarenal flow and 21% decrease in upper body flow [50]. Capacitances for the outflow boundary conditions were recalculated using the new waveforms and physiological exercise blood pressures [51].

The models were meshed using linear tetrahedral elements with a maximum edge size of 500 μm according to the results of previous mesh independence studies [11], resulting in final mesh sizes of $\mathcal{O}(10\text{M})$ elements. Simulations were run to convergence as determined by periodicity of the pressure waves. Only the five cardiac cycles following convergence were retained for postprocessing. These five cycles were repeated periodically for the platelet activation computations that spanned beyond five cycles.

2.2 Lagrangian Approach. The Lagrangian approach for the measurement of platelet activation was based on the modeling of individual platelets as infinitesimal particles [52]. Particle trajectories were governed by

$$\dot{\mathbf{x}}(t) = \mathbf{u}(\mathbf{x}, t) \tag{1}$$

where $\mathbf{u}$ was the fluid field velocity obtained from CFD.

A domain of interest Ω was defined to encompass the entire aneurysmal region (Fig. 1). Particles were released at the inlet plane in a manner that ensured a uniform influx [53]. Namely, particles were initially seeded uniformly across the inlet plane with 200 μm spacing. Subsequently, the reseeding rate at each location was determined by the local flow rate in space and time as to maintain a uniform influx concentration. In each case, several million particles were integrated resulting in particle concentrations of approximately 150,000 per cm^3 based on the results of a convergence study, which showed that 99.9th percentile AP levels changed by less than 1% when particle concentration was doubled. To isolate the effect of platelet activation within the aneurysm, particles were tracked from their initial seeding locations until they exited Ω.

The Lagrangian AP ϕ_L for each particle was based on a linear stress-exposure time model

$$\phi_L(\mathbf{x}_0, t_0) = \sum_{i=1}^{N} \tau(\mathbf{x}(t_i; \mathbf{x}_0, t_0), t_i)\Delta t \tag{2}$$

where N is the total number of time steps the particle spends in Ω, Δt is the length of each time step used for integration of Eq. (1), and τ is a scalar stress value defined below. Particles were continuously seeded and tracked until peak values of ϕ_L became periodic, at which point quantification of AP was performed as described below.

Shadden and Hendababi [33] proposed a metric for platelet AP based on the Frobenius norm of the rate of deformation tensor

[1] simtk.org/home/simvascular

$$\|\mathbf{e}\|_F = \sqrt{\mathrm{tr}(\mathbf{e}^{\mathrm{T}}\mathbf{e})} = \sqrt{\sum_{i=1}^{3}\sum_{j=1}^{3} e_{ij}^2} \tag{3}$$

where $\mathbf{e}$ is the rate of deformation tensor, given by

$$\mathbf{e}(\mathbf{x},t) = \frac{1}{2}\left(\nabla\mathbf{u}(\mathbf{x},t) + \nabla\mathbf{u}(\mathbf{x},t)^{\mathrm{T}}\right) \tag{4}$$

According to the Newtonian approximation, the deviatoric stress tensor in a fluid is given by $\mathbf{s} = 2\mu\mathbf{e}$, where μ is the dynamic viscosity. Incorporating the Frobenius norm, and setting the value of τ in an arbitrary flow equal to the stress in simple shear, the scalar stress becomes

$$\tau(\mathbf{x},t) = \sqrt{2}\mu\|\mathbf{e}(\mathbf{x},t)\|_F \tag{5}$$

It can be shown that in an incompressible fluid this scalar stress value is equivalent to the von Mises stress-based metric used by other researchers in platelet AP studies [25,29,35,54].

Equation (2) does not provide a meaningful visualization of the results, due to the dependence of ϕ on initial location and time of particle release. It is desirable to have a measure of AP that can distinguish regions prone to higher levels of activation. To enable calculation of such a measure within the Lagrangian framework, the aneurysmal domain Ω was divided into subdomains Ω_i corresponding to the cells used in the finite element analysis, such that

$$\Omega = \bigcup_{i=1}^{N_\Omega} \Omega_i \tag{6}$$

where N_Ω is the total number of subdomains. Once convergence of peak values was obtained, time-averaged AP was then calculated over one cardiac cycle for each subdomain as an average of the contributions of all platelets visiting the subdomain

$$\bar{\phi}_L(\Omega_i) = \frac{1}{N_t}\sum_{j=1}^{N_t}\sum_{k\in S}\frac{1}{|S|}\tilde{\phi}\left(t_j;\mathbf{x}_0^k,t_0^k\right) \tag{7}$$

where $S(\Omega_i,t_j) = \{k|\mathbf{x}(t_j;\mathbf{x}_0^k,t_0^k)\in\Omega_i\}$ is the set of particles in Ω_i at time t_j, $|S|$ is the size of this set, N_t is the number of time steps in the cycle, and $\tilde{\phi}(t_j;\mathbf{x}_0^k,t_0^k)$ is the activation level for particle k from time t_0 until time t_j.

2.3 Eulerian Approach. In the Eulerian approach, platelet activation level ϕ_{E} was modeled as a continuum quantity using a reaction–advection–diffusion equation

$$\frac{\partial\phi_{\mathrm{E}}(\mathbf{x},t)}{\partial t} = -\mathbf{u}(\mathbf{x},t)\cdot\nabla\phi_{\mathrm{E}}(\mathbf{x},t) + \nabla\cdot\kappa\nabla\phi_{\mathrm{E}}(\mathbf{x},t) + \eta(\mathbf{x},t) \tag{8}$$

where κ is platelet diffusivity and $\eta(\mathbf{x},t)$ is the local platelet activation rate. For the linear stress-exposure time model, $\eta(\mathbf{x},t) = \tau(\mathbf{x},t)$. To isolate the effect of platelet activation within the aneurysm, the local activation rate was defined as

$$\eta(\mathbf{x},t) = \begin{cases} \tau(\mathbf{x},t), & \mathbf{x}\in\Omega \\ 0, & \mathbf{x}\notin\Omega \end{cases} \tag{9}$$

The value of κ for platelets depends not only on the Brownian motion of the platelets, but also on the influence of shear rate and red blood cell interactions [40]. Even with upper-bounds estimates for κ, the Peclet numbers in the regions of interest in this study were on the order of 10^6–10^7, indicating diffusion has a negligible role. Indeed, preliminary studies confirmed that realistic levels for platelet diffusion had no perceptible influence on results, so the value of κ was set to zero for simplification.

Equation (8) was solved using a finite element method [55] over the same computational mesh as used for the CFD calculations. A Dirichlet boundary condition of $\phi_{\mathrm{E}} = 0$ was imposed at the supraceliac aorta inlet. A Neumann zero flux boundary condition was applied at all other surfaces. The homogenous Neumann boundary condition was also applied at the flow outlets, as it was assumed that these boundaries were far enough away from the activation region such that $\nabla\phi_{\mathrm{E}}$ was negligibly small. An initial condition of $\phi_{\mathrm{E}}(\mathbf{x},0) = 0$ was imposed throughout the domain.

To compare statistics between the Lagrangian and Eulerian methods, nodal values from the Eulerian method were interpolated to cell centers, to provide cell-based field data

$$\phi_{\mathrm{E}}(\Omega_i,t) = \phi_{\mathrm{E}}(\mathbf{x}_i^c,t) \tag{10}$$

where $\mathbf{x}_i^c$ is the center of subdomain Ω_i. Time-averaged AP was then calculated over one cardiac cycle (once solution converged) as

$$\bar{\phi}_{\mathrm{E}}(\Omega_i) = \frac{1}{N_t}\sum_{j=1}^{N_t}\phi_{\mathrm{E}}(\Omega_i,t_j) \tag{11}$$

so that both Eulerian (11) and Lagrangian (7) time-averaged AP fields were defined at each finite element Ω_i.

2.4 Additional Models. A power law model for AP of the form

$$\phi_{pl} = \int_{t_0}^{t}\tau^{\alpha}d\xi \tag{12}$$

was applied to one patient to investigate dependence of the results on the AP model. A value of $\alpha = 2.28$ (all units centimeter-gram-second (cgs)) was chosen to allow comparison to the Hellums locus [20]. AP was computed in the Lagrangian method as

$$\phi_{pl,\mathrm{L}}(t) = \sum_{i=1}^{N_t}\tau(\mathbf{x},t_i)^{\alpha}\Delta t \tag{13}$$

in place of Eq. (2), and in the Eulerian method using

$$\eta_{pl,\mathrm{E}}(\mathbf{x},t) = \tau(\mathbf{x},t)^{\alpha} \tag{14}$$

in place of Eq. (9).

Additionally, the Soares model [29] was implemented within the Eulerian framework. The contribution of the stress rate term was assumed to be negligibly small, so the reaction term for this model took the form

$$\eta_{\mathrm{S}} = (1-\phi_{\mathrm{s}})\left(S_{\mathrm{r}}\phi\phi_{\mathrm{s}} + C^{\frac{1}{\beta}}\beta\phi_{\mathrm{s}}^{\frac{\beta-1}{\beta}}\tau^{\frac{\alpha}{\beta}}\right) \tag{15}$$

where η_{S} represents the reaction term for ϕ_{s}, the fraction of activated platelets, and ϕ is the previously determined linear stress-exposure time AP. All other terms are constants, and were assigned the values experimentally determined by Soares et al. [29] (all units cgs): $S_{\mathrm{r}} = 1.5701\times10^{-7}$, $C = 1.4854\times10^{-7}$, $\alpha = 1.4854$, and $\beta = 1.4401$. This model requires an initial concentration of activated platelets. The equilibrium background level of activated platelets has been estimated at between 1% and 20% [40]; a value of 5% was tested in this study. This value for ϕ_{S} was assigned as an initial condition throughout the computational domain, as well as a Dirichlet boundary condition on the supraceliac aorta inlet.

2.5 Statistical Methods. Volume-weighted probability density and complementary cumulative distribution functions (CCDF) were

Table 1 Number of cardiac cycles to convergence for Lagrangian and Eulerian methods

	Patient	1		2		3		4		5	
	Condition	R	E	R	E	R	E	R	E	R	E
Cycles	Lagrangian	16.3	13.2	22.0	9.1	20.2	10.1	50.4	15	21.1	8.8
	Eulerian	4.3	3.4	6.6	1.7	7.6	1.9	16.8	4.9	6.8	1.8

Table 2 Peak, 99th percentile, and time-averaged primary mode values for AP from linear stress-exposure time model, under rest (R) and exercise (E) conditions. All results are in units of dyn s cm^{-2}.

	Patient	1		2		3		4		5	
	Condition	R	E	R	E	R	E	R	E	R	E
Peak	Lagrangian	34.8	52.2	35.8	38.9	34.7	35.5	50.0	33.8	48.4	41.2
	Eulerian	6.4	9.4	7.6	7.9	7.4	8.3	10.2	7.3	9.3	9.5
99%	Lagrangian	8.5	13.3	9.6	10.5	8.8	8.8	7.6	8.6	14.5	13.1
Mode	Lagrangian	2.0	0	2.9	3.6	1.9	2.0	1.6	1.6	5.1	4.7
	Eulerian	1.9	0	3.0	3.4	1.9	1.8	1.8	1.5	5.4	4.5

calculated from the time-averaged AP results to facilitate a quantitative comparison between the Lagrangian and Eulerian methods. All reported p-values were obtained using two-sided paired Student's t-tests.

3 Results

Table 1 lists the number of cardiac cycles to convergence of peak AP for each patient. In all cases, the Lagrangian method took more than 2.5 × more cycles to converge than the Eulerian method. The time to convergence for the rest condition was more than twice as long as the exercise condition for all patients with the exception of patient 1. Patient 5, rest condition, required more than twice as long as any other case to reach convergence with both the Lagrangian and Eulerian methods.

AP results using the linear stress-exposure time model are listed in Table 2. Peak values were 387% ± 43% (mean ± SD) higher when using the Lagrangian method ($p < 0.001$), however the much higher peak values in the Lagrangian method were limited to relatively few platelets. For example, the 99th percentile values were only 25% ± 22% ($p = 0.02$) higher with the Lagrangian method. Moderate exercise caused a 3% ± 31% ($p = 0.94$) increase in peak AP based on the Lagrangian results, and a 7% ± 27% ($p = 0.76$) increase based on the Eulerian results. Both methods obtained similar primary modes for all patients. Excluding the results from patient 1, exercise condition, which had a mode at zero, the Lagrangian method measured primary modes 0% ± 6% ($p = 0.92$) higher than the Eulerian method.

The power law model was applied to patient 1 only. This model showed that exercise conditions increased peak AP from 540 to 11998 using the Lagrangian method, and from 333 to 1103 using the Eulerian method (all units cgs). The 99th percentile Lagrangian values were 111 and 1108 for rest and exercise, respectively.

Examination of the PDF (Fig. 2) and CCDF (Fig. 3) for $\bar{\phi}$ revealed relative agreement between the results of the two methods with both the linear and power law models. Results were qualitatively similar between rest and exercise conditions, except for patient 1 who demonstrated a substantial increase in probability of elevated AP levels during exercise versus rest, especially with the power law model. It is also interesting to note that the PDF for patient 5 was distinctly bimodal, perhaps corresponding to the apparent bilobed aneurysm.

Figures 4–9 show volume renderings of time-averaged APs. The two methods show similar topological features for all patients, although peak values appear to be slightly higher with

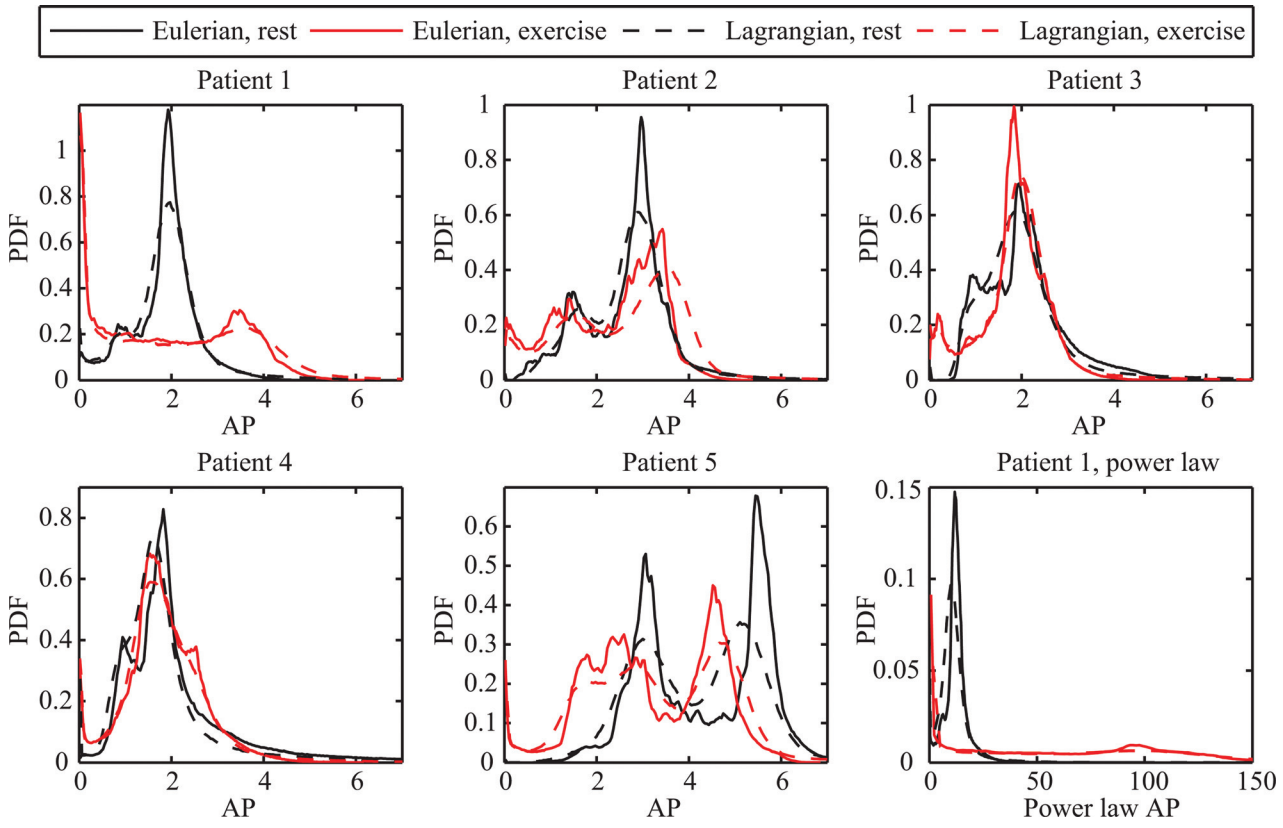

Fig. 2 PDF for time-averaged platelet AP. All results are based on linear stress-exposure time model except where noted, and in cgs units.

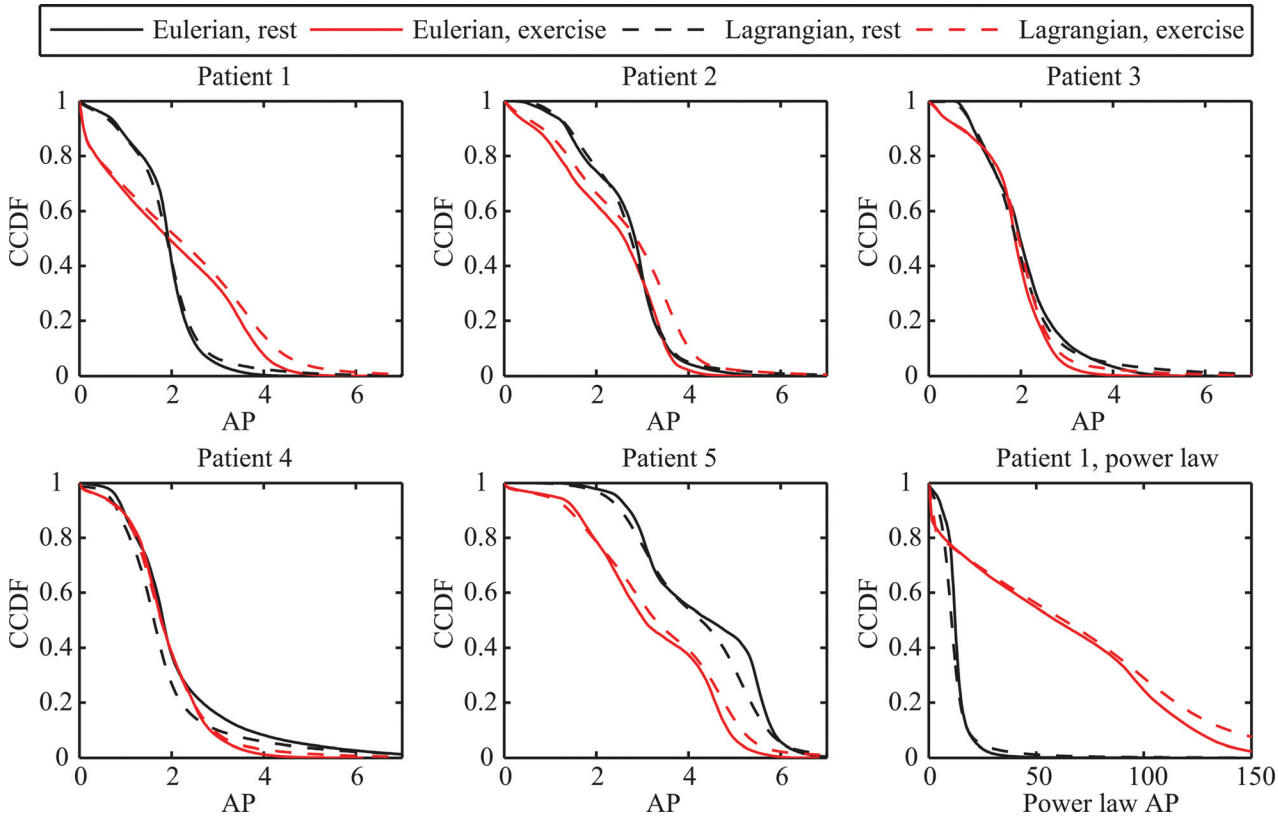

Fig. 3 CCDF for time-averaged platelet AP. All results are based on linear stress-exposure time model except where noted, and in cgs units.

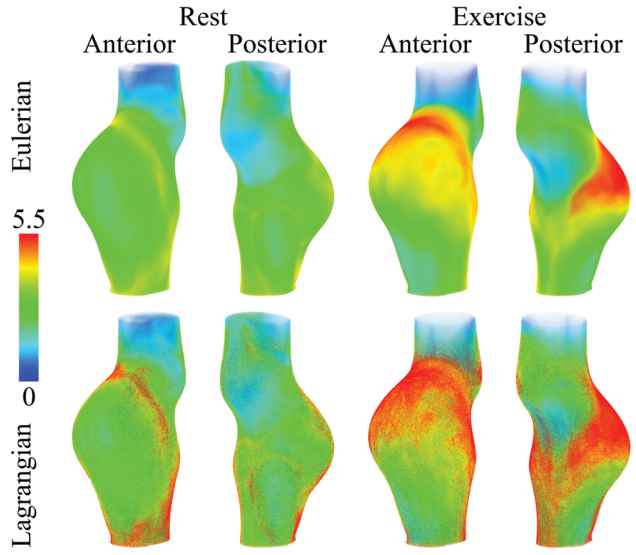

Fig. 4 Volume rendering of time-averaged AP (dyn s cm^{-2}) for patient 1, based on linear stress-exposure time model

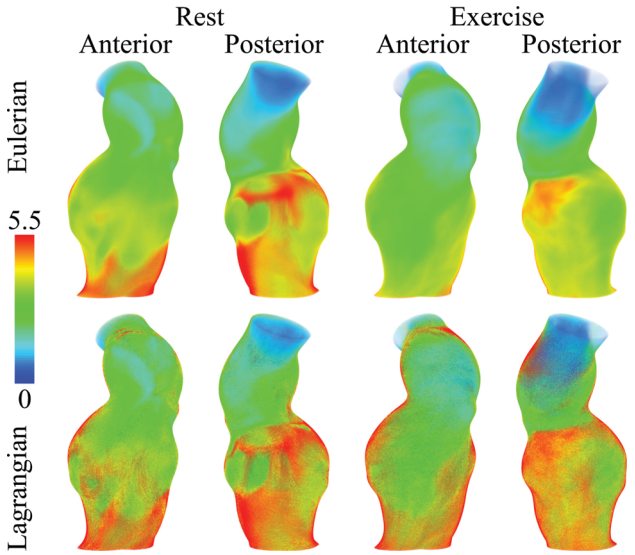

Fig. 5 Volume rendering of time-averaged AP (dyn s cm^{-2}) for patient 2, based on linear stress-exposure time model

the Lagrangian method consistent with results in Table 2. Regions of high AP seem to be quite coherent and localized in all patients. With the exception of patient 1, activation levels typically appeared higher on the distal half of the aneurysm.

4 Discussion

Herein we considered the stress-histories of particles passing through small to medium sized (3–5 cm dia.) AAA under both simulated rest and exercise flow conditions. These aneurysms were mostly thrombus free, and were of a size where thrombus burden typically begins to develop [56]. The maximum value for platelet AP in any patient, based on the linear stress-activation time model, was 52 dyn s cm^{-2}. While the Hellums et al. [20] locus does not show a linear relationship between threshold stress and exposure time, it can be used to establish a lower bound for AP threshold. At physiological levels of shear stress in aortic flows ($<$100 dyn s cm^{-2}), the Hellums locus gives an AP threshold of at least 10^4 dyn s cm^{-2}. This is orders of magnitude higher

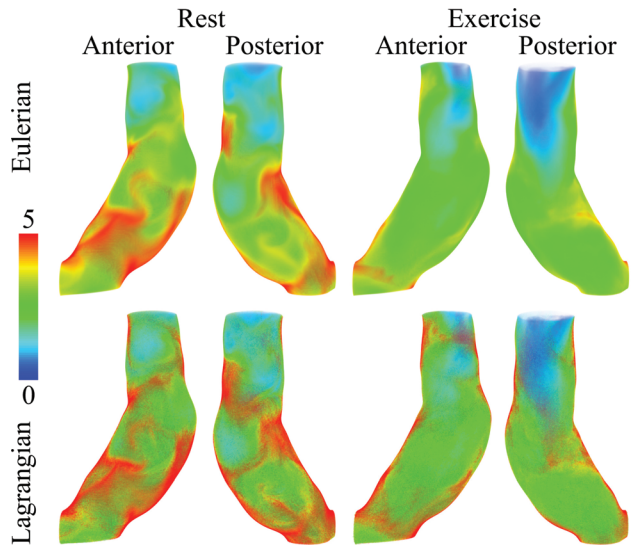

Fig. 6 Volume rendering of time-averaged AP (dyn s cm^{-2}) for patient 3, based on linear stress-exposure time model

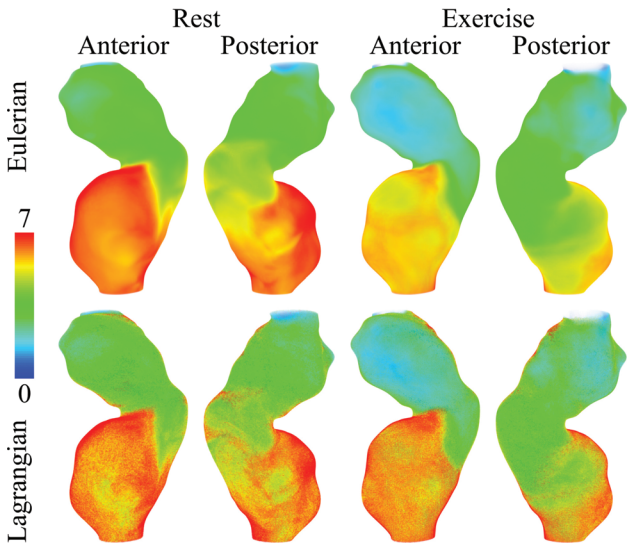

Fig. 8 Volume rendering of time-averaged AP (dyn s cm^{-2}) for patient 5, based on linear stress-exposure time model

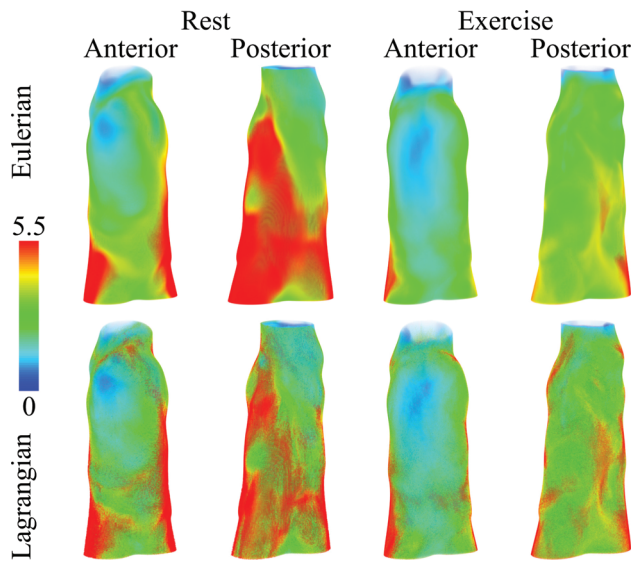

Fig. 7 Volume rendering of time-averaged AP (dyn s cm^{-2}) for patient 4, based on linear stress-exposure time model

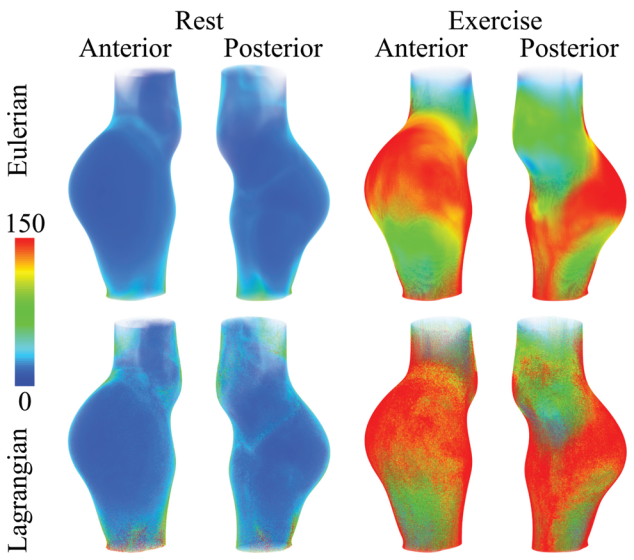

Fig. 9 Volume rendering of time-averaged power law AP (cgs units) for patient 1

than the values obtained in this study. Similar conclusions can be drawn from the power law model. The peak value obtained using the power law model was 1.2×10^5 (cgs units). This value can be compared to the Hellums locus, which gives a threshold of 3×10^6. Similarly, tests with the Soares model showed that levels of newly activated platelets within the aneurysm were less than 1% of background levels. These results indicate that—at least for the specific AAA geometries and flow conditions considered in this study—biomechanical platelet activation does not likely play a significant role in thrombus formation, and that other mechanisms such as biochemical activation should be considered.

Peak AP levels obtained using the Lagrangian method were significantly higher than their counterparts obtained using the Eulerian method. However, less than 1% of particles were the cause of this specific discrepancy, and otherwise the two distributions of activation level were in good agreement. Convergence of AP values was lower with the Lagrangian method, although this discrepancy was again limited to very few platelets, and the probability distribution functions converged much more quickly.

Because of the complexity of the flow field in AAA, particle trajectories are chaotic in nature. It is expected that there may be a small set of initial conditions whose trajectories have excessively long residence times, which is consistent with longer convergence times for the Lagrangian computations. Examples include those whose trajectory places them very close to the wall where velocity is near zero, or near invariant manifolds [57,58] that have accumulation points on the wall. Both cases are where deviatoric stress tends to be highest [33]. In theory, trajectories that have accumulation points on the wall can have infinite residence time, although these sets are zero measure. However, trajectories initialized very close to such zero measure sets can have similar "singular" behavior. This is less pronounced in the Eulerian method because the continuum model inherently smooths subgrid scale behavior, as well as adds numerical (and physical) diffusion. Likewise, this smoothing effect in the Eulerian method provides a higher concentration of platelets at the modal values; hence the concentrations at the modal values are consistently higher in the Eulerian method than Lagrangian method, as shown in Fig. 2.

While the Lagrangian method may better capture the accumulated stress histories of individual platelets, the validity of using an Eulerian continuum method to analyze biomechanical platelet activation depends on whether or not these extreme values are considered significant. Estimates from the literature for background levels of platelet activation under normal conditions range from 1% to 20% [40]. Since the main disparity between values obtained using the Lagrangian and Eulerian methods was limited to approximately 1% of all platelets, and otherwise the two distributions of activation level were in good agreement, it can be argued that even if the Eulerian method underestimates the activation level of a small number of platelets, this error is negligible compared to expected background levels of activated platelets.

Using the linear stress-exposure time model, peak activation levels for exercise conditions were all within 50% of the values obtained under rest conditions. With the power law model, exercise levels were up to 20 times higher. This difference emphasizes the dependance on model choice when stress duration and magnitude are competing influences, as is typically the case in cardiovascular flows. In nearly all regions of altered hemodynamic conditions, including aneurysms and stenoses, an increased flow rate will lead to higher shear stresses along with decreased residence times. The effect of this competition between stress duration and magnitude is complex and patient-specific, as indicated by the lack of a consistent trend between the rest and exercise results with the linear model. The purpose of this study is not to determine which AP model is "better," but rather to determine if either model would predict mechanical activation in physiologically realistic AAA flow conditions.

Analysis of AP in this work was limited to an isolated region of interest, i.e., the aneurysm. This may have led to an underestimation of actual integrated stress states on platelets inside the aneurysm, since platelets entering the aneurysm will have some previous stress history. Nonetheless, the goal of this study was to investigate the potential role of biomechanical platelet activation *within* AAA. Therefore the exclusion of prior stress history allowed for the isolation of these effects. Additionally, there is evidence that antithrombotic agents released from healthy endothelial tissue act to suppress platelet activation and adhesion outside of the aneurysm [14,59].

Both the Lagrangian and Eulerian models in this study assumed that blood was a continuum for purposes of deriving the velocity and rate of strain tensor fields. In reality, blood is a suspension of approximately 40% red blood cells. While the continuum approximation may provide an adequate description of the blood flow dynamics at the macroscale, using this information to attempt to resolve the local stresses exerted on individual platelets may introduce some error to the model. At this scale, the stresses are likely to include both viscous stresses from the plasma and local interaction forces with red blood cells. A continuum model is consistent with most platelet activation experiments, which are typically conducted using platelet-rich plasma in the absence of red blood cells. How these stresses correlate to those exerted on platelets under in vivo conditions in the presence of red blood cells is not well understood.

Blood was approximated as a Newtonian fluid even though blood is known to have complex rheology. The differences and tradeoffs between using a Newtonian versus non-Newtonian model in large artery flow simulations have been considered in several prior studies, and reviewed in Ref. [60]. We have tested non-Newtonian models in prior AAA flow modeling studies and have found that differences in the velocity field resulting from commonly employed rheological models are minor compared to differences in the velocity field resulting from inter-patient variation in aneurysm shape, volumetric flow, or heart rate. These differences have all been considered herein. Moreover, the results indicate that the accumulated stress histories were orders of magnitude lower than those generally expected to induce platelet activation. This finding is unlikely to change due to physiologic variations in rheology.

Particles were seeded uniformly across the inlet plane in the Lagrangian method. There is evidence that platelets congregate toward the walls of smaller blood vessels. In larger vessels, however, these effects are expected to be minimal [61] because the flow is complex and highly three-dimensional. In any case, the levels of AP in this study were orders of magnitude lower than the expected thresholds, and it is unlikely that the seeding distribution will affect this conclusion.

Acknowledgment

This work was supported by the NIH National Heart Lung and Blood Institute (Grant No. HL108272) and the National Science Foundation (Grant No. 1354541).

References

[1] Wolf, Y. G., Thomas, W. S., Brennan, F. J., Goff, W. G., Sise, M. J., and Bernstein, E. F., 1994, "Computed Tomography Scanning Findings Associated With Rapid Expansion of Abdominal Aortic Aneurysms," J. Vasc. Surg., **20**(4), pp. 529–538.
[2] Stenbaek, J., Kalin, B., and Swedenborg, J., 2000, "Growth of Thrombus May be a Better Predictor of Rupture Than Diameter in Patients With Abdominal Aortic Aneurysms," Eur. J. Vasc. Endovasc. Surg., **20**(5), pp. 466–469.
[3] Raut, S. S., Chandra, S., Shum, J., and Finol, E. A., 2013, "The Role of Geometric and Biomechanical Factors in Abdominal Aortic Aneurysm Rupture Risk Assessment," Ann. Biomed. Eng., **41**(7), pp. 1459–1477.
[4] Wilson, J. S., Virag, L., Di Achille, P., Karsaj, I., and Humphrey, J. D., 2013, "Biochemomechanics of Intraluminal Thrombus in Abdominal Aortic Aneurysms," ASME J. Biomech. Eng., **135**(2), p. 021011.
[5] Asbury, C. L., Ruberti, J. W., Bluth, E. I., and Peattie, R. A., 1995, "Experimental Investigation of Steady Flow in Rigid Models of Abdominal Aortic Aneurysms," Ann. Biomed. Eng., **23**(1), pp. 29–39.
[6] Bluestein, D., Dewanjee, M. K., Niu, L., and Schoephoerster, R. T., 1996, "Steady Flow in an Aneurysm Model: Correlation Between Fluid Dynamics and Blood Platelet Deposition," ASME J. Biomech. Eng., **118**(3), pp. 280–286.
[7] Egelhoff, C. J., Budwig, R. S., Elger, D. F., Khraishi, T. A., and Johansen, K. H., 1999, "Model Studies of the Flow in Abdominal Aortic Aneurysms During Resting and Exercise Conditions," J. Biomech., **32**(12), pp. 1319–1329.
[8] Salsac, A. V., Sparks, S. R., and Lasheras, J. C., 2004, "Hemodynamic Changes Occurring During the Progressive Enlargement of Abdominal Aortic Aneurysms," Ann. Vasc. Surg., **18**(1), pp. 14–21.
[9] Stamatopoulos, C., Mathioulakis, D. S., Papaharilaou, Y., and Katsamouris, A., 2011, "Experimental Unsteady Flow Study in a Patient-Specific Abdominal Aortic Aneurysm Model," Exp. Fluids, **50**(6), pp. 1695–1709.
[10] Biasetti, J., Gasser, T. C., Auer, M., Hedin, U., and Labruto, F., 2009, "Hemodynamics of the Normal Aorta Compared to Fusiform and Saccular Abdominal Aortic Aneurysms With Emphasis on a Potential Thrombus Formation Mechanism," Ann. Biomed. Eng., **38**(2), pp. 380–390.
[11] Les, A. S., Shadden, S. C., Figueroa, C. A., Park, J. M., Tedesco, M. M., Herfkens, R. J., Dalman, R. L., and Taylor, C. A., 2010, "Quantification of Hemodynamics in Abdominal Aortic Aneurysms During Rest and Exercise Using Magnetic Resonance Imaging and Computational Fluid Dynamics," Ann. Biomed. Eng., **38**(4), pp. 1288–1313.
[12] Arzani, A., and Shadden, S. C., 2012, "Characterization of the Transport Topology in Patient-Specific Abdominal Aortic Aneurysm Models," Phys. Fluids, **24**(8), p. 081901.
[13] Arzani, A., Les, A. S., Dalman, R. L., and Shadden, S. C., 2014, "Effect of Exercise on Patient Specific Abdominal Aortic Aneurysm Flow Topology and Mixing," Int. J. Numer. Methods Biomed. Eng., **30**(2), pp. 280–295.
[14] Biasetti, J., Hussain, F., and Gasser, T. C., 2011, "Blood Flow and Coherent Vortices in the Normal and Aneurysmatic Aortas: A Fluid Dynamical Approach to Intra-Luminal Thrombus Formation," J. R. Soc. Interface, **8**(63), pp. 1449–1461.
[15] Basciano, C., Kleinstreuer, C., Hyun, S., and Finol, E. A., 2011, "A Relation Between Near-Wall Particle-Hemodynamics and Onset of Thrombus Formation in Abdominal Aortic Aneurysms," Ann. Biomed. Eng., **39**(7), pp. 2010–2026.
[16] Arzani, A., Suh, G., Dalman, R. L., and Shadden, S. C., 2014, "A Longitudinal Comparison of Hemodynamics and Intraluminal Thrombus Deposition in Abdominal Aortic Aneurysms," Am. J. Physiol., **307**(12), pp. H1786–H1795.
[17] Brown, C. H., III, Lemuth, R. F., Hellums, J. D., Leverett, L. B., and Alfrey, C. P., 1975, "Response of Human Platelets to Shear Stress," Trans. Am. Soc. Artif. Intern. Organs, **21**(1), pp. 35–39.
[18] Ramstack, J. M., Zuckerman, L., and Mockros, L. F., 1979, "Shear-Induced Activation of Platelets," J. Biomech., **12**(2), pp. 113–125.
[19] Wurzinger, L. J., Opitz, R., Blasberg, P., and Schmid-Schonbein, H., 1985, "Platelet and Coagulation Parameters Following Millisecond Exposure to Laminar Shear Stress," Thromb. Haemostasis, **54**(2), pp. 381–386.
[20] Hellums, J. D., Peterson, D. M., Stathopoulos, N. A., Moake, J. L., and Giorgio, T. D., 1987, "Studies on the Mechanisms of Shear-Induced Platelet Activation," *Cerebral Ischemia and Hemorheology*, Springer, Berlin, Heidelburg, Germany, pp. 80–89.

[21] Giersiepen, M., Wurzinger, L. J., Opitz, R., and Reul, H., 1990, "Estimation of Shear Stress-Related Blood Damage in Heart Valve Prostheses—In Vitro Comparison of 25 Aortic Valves," Int. J. Artif. Organs, **13**(5), pp. 300–306.
[22] Bluestein, D., Niu, L., Schoephoerster, R. T., and Dewanjee, M. K., 1997, "Fluid Mechanics of Arterial Stenosis: Relationship to the Development of Mural Thrombus," Ann. Biomed. Eng., **25**(2), pp. 344–356.
[23] Einav, S., and Bluestein, D., 2004, "Dynamics of Blood Flow and Platelet Transport in Pathological Vessels," Ann. N. Y. Acad. Sci., **1015**(1), pp. 351–366.
[24] Nobili, M., Sheriff, J., Morbiducci, U., Redaelli, A., and Bluestein, D., 2008, "Platelet Activation Due to Hemodynamic Shear Stresses: Damage Accumulation Model and Comparison to In Vitro Measurements," ASAIO J., **54**(1), pp. 64–72.
[25] Wu, J., Paden, B. E., Borovetz, H. S., and Antaki, J. F., 2009, "Computational Fluid Dynamics Analysis of Blade Tip Clearances on Hemodynamic Performance and Blood Damage in a Centrifugal Ventricular Assist Device," Artif. Organs, **34**(5), pp. 402–411.
[26] Wu, J., Yun, B. M., Fallon, A. M., Hanson, S. R., Aidun, C. K., and Yoganathan, A. P., 2010, "Numerical Investigation of the Effects of Channel Geometry on Platelet Activation and Blood Damage," Ann. Biomed. Eng., **39**(2), pp. 897–910.
[27] Grigioni, M., Daniele, C., Morbiducci, U., D'Avenio, G., Di Benedetto, G., and Barbaro, V., 2004, "The Power-Law Mathematical Model for Blood Damage Prediction: Analytical Developments and Physical Inconsistencies," Artif. Organs, **28**(5), pp. 467–475.
[28] Grigioni, M., Morbiducci, U., D'Avenio, G., Benedetto, G. D., and Gaudio, C. D., 2005, "A Novel Formulation for Blood Trauma Prediction by a Modified Power-Law Mathematical Model," Biomech. Modell. Mechanobiol., **4**(4), pp. 249–260.
[29] Soares, J. S., Sheriff, J., and Bluestein, D., 2013, "A Novel Mathematical Model of Activation and Sensitization of Platelets Subjected to Dynamic Stress Histories," Biomech. Modell. Mechanobiol., **12**(6), pp. 1127–1141.
[30] Sheriff, J., Soares, J. S., Xenos, M., Jesty, J., and Bluestein, D., 2013, "Evaluation of Shear-Induced Platelet Activation Models Under Constant and Dynamic Shear Stress Loading Conditions Relevant to Devices," Ann. Biomed. Eng., **41**(6), pp. 1279–1296.
[31] Song, X., Throckmorton, A. L., Wood, H. G., Antaki, J. F., and Olsen, D. B., 2003, "Computational Fluid Dynamics Prediction of Blood Damage in a Centrifugal Pump," Artif. Organs, **27**(10), pp. 938–941.
[32] Tambasco, M., and Steinman, D. A., 2003, "Path-Dependent Hemodynamics of the Stenosed Carotid Bifurcation," Ann. Biomed. Eng., **31**(9), pp. 1054–1065.
[33] Shadden, S. C., and Hendabadi, S., 2012, "Potential Fluid Mechanic Pathways of Platelet Activation," Biomech. Modell. Mechanobiol., **12**(3), pp. 467–474.
[34] Chan, W. K., Wong, Y. W., Ding, Y., Chua, L. P., and Yu, S. C. M., 2002, "Numerical Investigation of the Effect of Blade Geometry on Blood Trauma in a Centrifugal Blood Pump," Artif. Organs, **26**(9), pp. 785–793.
[35] Alemu, Y., and Bluestein, D., 2007, "Flow-Induced Platelet Activation and Damage Accumulation in a Mechanical Heart Valve: Numerical Studies," Artif. Organs, **31**(9), pp. 677–688.
[36] Dumont, K., Vierendeels, J., Kaminsky, R., van Nooten, G., Verdonck, P., and Bluestein, D., 2007, "Comparison of the Hemodynamic and Thrombogenic Performance of Two Bileaflet Mechanical Heart Valves Using a CFD/FSI Model," ASME J. Biomech. Eng., **129**(4), pp. 558–565.
[37] Yun, B. M., Wu, J., Simon, H. A., Arjunon, S., Sotiropoulos, F., Aidun, C. K., and Yoganathan, A. P., 2012, "A Numerical Investigation of Blood Damage in the Hinge Area of Aortic Bileaflet Mechanical Heart Valves During the Leakage Phase," Ann. Biomed. Eng., **40**(7), pp. 1468–1485.
[38] Soares, J. S., Gao, C., Alemu, Y., Slepian, M., and Bluestein, D., 2013, "Simulation of Platelets Suspension Flowing Through a Stenosis Model Using a Dissipative Particle Dynamics Approach," Ann. Biomed. Eng., **41**(11), pp. 2318–2333.
[39] Born, G. V. R., and Cross, M. J., 1963, "The Aggregation of Blood Platelets," J. Physiol., **168**(1), pp. 178–195.
[40] Sorensen, E. N., Burgreen, G. W., Wagner, W. R., and Antaki, J. F., 1999, "Computational Simulation of Platelet Deposition and Activation: I. Model Development and Properties," Ann. Biomed. Eng., **27**(4), pp. 436–448.
[41] Sorensen, E. N., Burgreen, G. W., Wagner, W. R., and Antaki, J. F., 1999, "Computational Simulation of Platelet Deposition and Activation: II. Results for Poiseuille Flow Over Collagen," Ann. Biomed. Eng., **27**(4), pp. 449–458.
[42] Anand, M., Rajagopal, K., and Rajagopal, K. R., 2003, "A Model Incorporating Some of the Mechanical and Biochemical Factors Underlying Clot Formation and Dissolution in Flowing Blood," J. Theor. Med., **5**(3–4), pp. 183–218.
[43] Leiderman, K., and Fogelson, A. L., 2010, "Grow With the Flow: A Spatial–Temporal Model of Platelet Deposition and Blood Coagulation Under Flow," Math. Med. Biol., **28**(1), pp. 47–84.
[44] Leiderman, K., and Fogelson, A. L., 2013, "The Influence of Hindered Transport on the Development of Platelet Thrombi Under Flow," Bull. Math. Biol., **75**(8), pp. 1255–1283.
[45] Dalman, R. L., Tedesco, M. M., Myers, J., and Taylor, C. A., 2006, "AAA Disease: Mechanism, Stratification, and Treatment," Ann. N. Y. Acad. Sci., **1085**(1), pp. 92–109.
[46] Dua, M. M., and Dalman, R. L., 2010, "Hemodynamic Influences on Abdominal Aortic Aneurysm Disease: Application of Biomechanics to Aneurysm Pathophysiology," Vasc. Pharmacol., **53**(1–2), pp. 11–21.
[47] Suh, G., Les, A. S., Tenforde, A. S., Shadden, S. C., Spilker, R. L., Yeung, J. J., Cheng, C. P., Herfkens, R. J., Dalman, R. L., and Taylor, C. A., 2011, "Hemodynamic Changes Quantified in Abdominal Aortic Aneurysms With Increasing Exercise Intensity Using MR Exercise Imaging and Image-Based Computational Fluid Dynamics," Ann. Biomed. Eng., **39**(8), pp. 2186–2202.
[48] Taylor, C. A., Hughes, T. J., and Zarins, C. K., 1998, "Finite Element Modeling of Blood Flow in Arteries," Comput. Methods Appl. Mech. Eng., **158**(1–2), pp. 155–196.
[49] Jansen, K. E., Whiting, C. H., and Hulbert, G. M., 2000, "A Generalized-α Method for Integrating the Filtered Navier–Stokes Equations With a Stabilized Finite Element Method," Comput. Methods Appl. Mech. Eng., **190**(3–4), pp. 305–319.
[50] Cheng, C. P., Herfkens, R. J., and Taylor, C. A., 2003, "Abdominal Aortic Hemodynamic Conditions in Healthy Subjects Aged 50–70 at Rest and During Lower Limb Exercise: In Vivo Quantification Using MRI," Atherosclerosis, **168**(1), pp. 323–331.
[51] Montain, S. J., Jilka, S. M., Ehsani, A. A., and Hagberg, J. M., 1988, "Altered Hemodynamics During Exercise in Older Essential Hypertensive Subjects," Hypertension, **12**(5), pp. 479–484.
[52] Shadden, S. C., and Arzani, A., 2015, "Lagrangian Postprocessing of Computational Hemodynamics," Ann. Biomed. Eng., **43**(1), pp. 41–58.
[53] Lonyai, A., Dubin, A. M., Feinstein, J. A., Taylor, C. A., and Shadden, S. C., 2010, "New Insights Into Pacemaker Lead-Induced Venous Occlusion: Simulation-Based Investigation of Alterations in Venous Biomechanics," Cardiovasc. Eng., **10**(2), pp. 84–90.
[54] Apel, J., Paul, R., Klaus, S., Siess, T., and Reul, H., 2001, "Assessment of Hemolysis Related Quantities in a Microaxial Blood Pump by Computational Fluid Dynamics," Artif. Organs, **25**(5), pp. 341–347.
[55] Esmaily-Moghadam, M., Hsia, T., and Marsden, A. L., 2013, "A Non-Discrete Method for Computation of Residence Time in Fluid Mechanics Simulations," Phys. Fluids, **25**(11), p. 110802.
[56] Behr-Rasmussen, C., Grondal, N., Bramsen, M., Thomsen, M., and Lindholt, J., 2014, "Mural Thrombus and the Progression of Abdominal Aortic Aneurysms: A Large Population-Based Prospective Cohort Study," Eur. J. Vasc. Endovasc. Surg., **48**(3), pp. 301–307.
[57] Shadden, S. C., and Taylor, C. A., 2008, "Characterization of Coherent Structures in the Cardiovascular System," Ann. Biomed. Eng., **36**(7), pp. 1152–1162.
[58] Shadden, S. C., 2011, "Lagrangian Coherent Structures," *Transport and Mixing in Laminar Flows: From Microfluidics to Oceanic Currents*, Wiley-VCH, Weinheim, Germany.
[59] Cohen, R. A., Shepherd, J. T., and Vanhoutte, P. M., 1983, "Inhibitory Role of the Endothelium to the Response of Isolated Coronary Arteries to Platelets," Science, **221**(4607), pp. 273–274.
[60] Steinman, D. A., 2012, "Assumptions in Modelling of Large Artery Hemodynamics," *Modeling of Physiological Flows*, D. Ambrosi, A. Quarteroni, and G. Rozza, eds., Vol. 5, Springer, Milan, Italy, pp. 1–18.
[61] Biasetti, J., Spazzini, P. G., Hedin, U., and Gasser, T. C., 2014, "Synergy Between Shear-Induced Migration and Secondary Flows on Red Blood Cells Transport in Arteries: Considerations on Oxygen Transport," J. R. Soc. Interface, **12**(104), p. 20140403.